Large-eddy simulation of gas turbine combustors

By Krishnan Mahesh, George Constantinescu AND Parviz Moin

1. Motivation and objectives

The objective of this study is to develop tools to perform large-eddy simulation (LES) of turbulent flows in realistic engineering configurations. Of particular interest is the flow inside gas-turbine combustors. LES is an attractive approach for these flows, which are at relatively lower Reynolds numbers than external flows, and involve scalar mixing as a central component. This report discusses our progress towards developing a numerical algorithm and solver for this purpose. As outlined in last year's report (Mahesh *et al.* Annual Research Briefs 1999), we have developed a conservative numerical algorithm that staggers the dependent variables to simulate incompressible flow on unstructured grids. Our report last year outlined the algorithm as well as some details of its implementation on parallel platforms. It was noted that the algorithm was applicable to hybrid elements, the data structures used compressed storage formats to reduce memory use, a grid reordering technique was developed, and validation simulations were just being initiated.

2. Accomplishments

Our progress in the last year is as follows:

- A more efficient version of the constant density algorithm was derived for hybrid grids.
- Severe memory bottlenecks in the pre-processor part of the solver were removed. The pre-processor was rewritten to store data out of core; as a result, memory requirements of the order of gigabytes were reduced to the order of megabytes.
- The solver was validated for a variety of steady and unsteady flows.
- Simulations in a combustor geometry provided by Pratt & Whitney geometry were initiated; the unsteady flow in a subset of the overall geometry was simulated; the simulations retained the geometrical complexities of the full configuration.
- The dynamic Smagorinsky model for LES was extended to unstructured grids and implemented.
- The algorithm was extended to low Mach number, variable density flows; validation is in progress.

2.1. *Algorithm improvements*

2.1.1. *Base algorithm*

Recall that the constant density algorithm stores pressure at the centroids of the elements and velocity at their faces. As shown in Fig. 1, only one component of velocity is stored and advanced in time; the other two components are reconstructed. The velocity component v_n satisfies

$$\frac{\partial v_n}{\partial t} - (\vec{u} \times \vec{\omega}) \cdot \vec{n} + \frac{\partial}{\partial n}\left(\frac{\vec{u} \cdot \vec{u}}{2}\right) = -\frac{1}{\rho}\frac{\partial p}{\partial n} + \nu \left(\nabla^2 \vec{u}\right) \cdot \vec{n}. \tag{2.1}$$

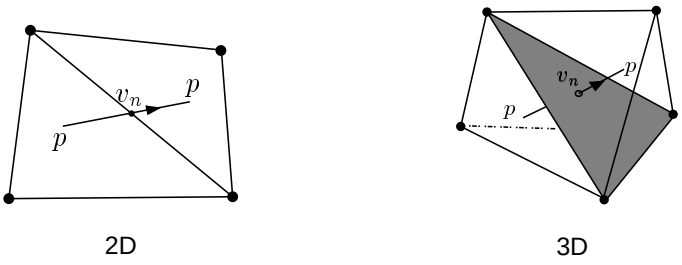

FIGURE 1. Positioning of variables in staggered algorithm.

Note that the convection term is written in terms of velocity and vorticity. The pressure-projection approach is used to ensure that the velocity field is discretely divergence-free; the resulting Poisson equation is solved using the conjugate gradient method with diagonal preconditioning. As shown in Fig. 1, v_n is not necessarily aligned with the face normal. As a result, the projection step involves the tangential velocities, which have to be reconstructed at every iteration. A more efficient formulation was therefore derived — the face normal velocity is now stored at the face centroid. Storing the normal component makes the projection step cheaper, while storing velocities at the centroid makes flux calculations more accurate.

2.1.2. *The dynamic model*

The dynamic Smagorinsky model (Germano *et al.* 1991) was extended to unstructured grids. Recall that the LES equations are

$$\frac{\partial \overline{u_i}}{\partial t} + \frac{\partial \overline{u}_i \overline{u}_j}{\partial x_j} = -\frac{\partial \phi}{\partial x_i} + \frac{1}{Re}\frac{\partial^2 \overline{u}_i}{\partial x_j x_j} - \frac{\partial q_{ij}}{\partial x_j} \tag{2.2}$$

where q_{ij} denotes the anisotropic part of the subgrid-scale stress, $\overline{u_i u_j} - \overline{u}_i \overline{u}_j$, and the overbar indicates filtered variables. Note that the above equation can equivalently be written with the convection term in rotational form.

The details of the dynamic modeling procedure may be found elsewhere and are not repeated here. We only note that the Smagorinsky model assumes that

$$q_{ij} = -2C\overline{\Delta}^2 |\overline{S}| \overline{S}_{ij} \tag{2.3}$$

where $\overline{S}_{ij}$ denotes the filtered strain-rate tensor. Application of the dynamic procedure using the least-squares approach (Lilly 1992) yields the following expression for C:

$$C\overline{\Delta}^2 = -\frac{1}{2}\frac{L_{ij}M_{ij}}{M_{kl}M_{kl}} \tag{2.4}$$

where

$$L_{ij} = \widehat{\overline{u}_i \overline{u}_j} - \widehat{\overline{u}}_i \widehat{\overline{u}}_j \tag{2.5}$$

and

$$M_{ij} = \left(\widehat{\overline{\Delta}}/\overline{\Delta}\right)^2 |\widehat{\overline{S}}| \widehat{\overline{S}}_{ij} - \widehat{|\overline{S}| \overline{S}_{ij}} \tag{2.6}$$

The dynamic procedure requires definition of a test-filter and the ratio of test to grid filter widths. The ratio of filter widths is commonly assumed to be 2; we do the same. We define the filter width at the faces of the grid as $V^{1/3}$ where V denotes the average of the volumes of the elements that straddle the face. This yields a filter width of $(\Delta_x \Delta_y \Delta_z)^{1/3}$ for a Cartesian grid. The test filter is assumed to be a top-hat filter

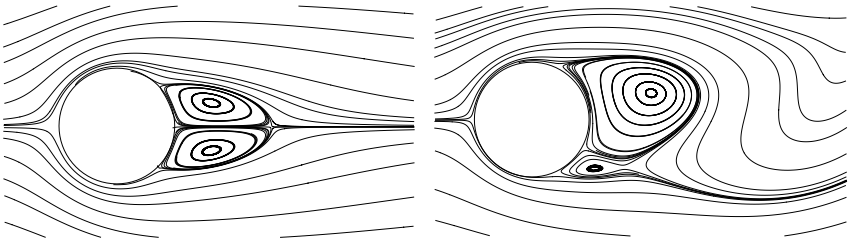

(*a*) (*b*)

FIGURE 2. Streamlines in the immediate vicinity of the cylinder. (*a*) : $Re = 20$, (*b*) : $Re = 100$.

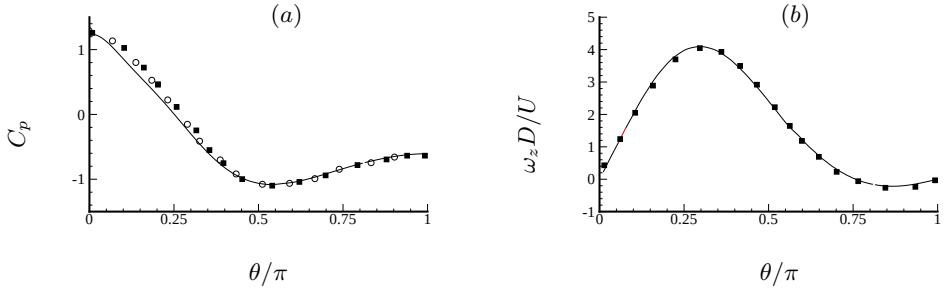

FIGURE 3. The vorticity and pressure coefficient (C_p) on the cylinder surface at $Re = 20$ are compared to experimental data. The solid lines are from the calculations, while the symbols are experimental data from Nieuwstadt & Keller (1973). (*a*): C_p, (*b*): vorticity.

and uses information from the neighboring volumes to obtain test-filtered values of the velocity at the faces. In practice, the dynamic model constant C is usually averaged over homogeneous directions, should such directions be present. Other approaches have been proposed for flows without homogeneous directions; e.g. Ghosal *et al.* (1994), Meneveau *et al.* (1996). Ghosal's approach requires solution of a variational problem and was successfully applied to flow over a backstep by Akselvoll & Moin (1995). The Lagrangian averaging proposed by Meneveau *et al.* (1996) has been successfully applied to channel flow but can exhibit sensitivity to the Lagrangian averaging time (D. You, private communication). In this report, we have chosen to filter the dynamic model coefficient in space instead of Lagrangian averaging. This implementation of the dynamic model is considered preliminary; the rationale for test-filtering the coefficients is that spatial filtering is consistent with the assumption in the dynamic procedure that the model coefficient does not vary over the test filter width.

2.1.3. *Variable density flow*

The constant density algorithm has been extended to variable density flow in the low Mach number limit. The dependent variable is now ρv_n instead of v_n, and the convection term is rewritten in terms of $\rho\vec{u}$ and its curl. Again, a pressure-projection approach is used to enforce the continuity equation. The energy equation may either be solved for, or temperature may be obtained by mapping from the scalars. Validation is in progress and is composed of two parts—evolving the scalars for constant density flow and evolving the variable density equations while specifying the density, and combining the two. The first two validations have been completed; similar computations in other simple laminar flows were performed.

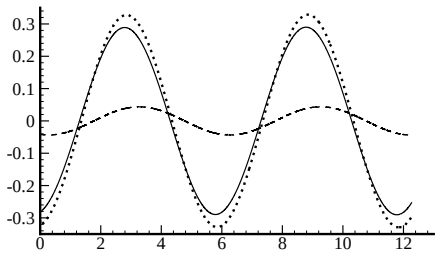

FIGURE 4. Lift coefficients at $Re = 100$. ——— (C_{l_p}), – – – (C_{l_v}), ····· (C_l). The subscripts p and v stand for contributions from pressure and viscosity respectively.

2.2. *Results*

Several computations were carried out to validate the numerical method. Some of these are discussed below.

2.2.1. *Flow over a cylinder*

The flow over a cylinder has been studied extensively by both experiments and computations. The flow is sensitive to Reynolds number, has attached and separated regions, and exhibits steady and unsteady regimes. It was therefore used for validation. Four simulations are planned: direct numerical simulation at $Re = 20, Re = 100, Re = 300$, and LES at $Re = 3900$. The first two calculations are completed and are reported here, while the latter two are in progress. Note that the flow at $Re = 20$ is two-dimensional and steady, that at $Re = 100$ it is two-dimensional and unsteady, while those at $Re = 300$ and 3900 are three-dimensional and unsteady. Regardless of the regime and dimensionality of the flow, all simulations reported solve the three-dimensional unsteady equations.

Figure 2 shows streamlines in the immediate vicinity of the cylinder at $Re = 20$ and 100. The asymmetry in the presence of shedding is apparent. Quantitative validation is provided in Figs. 3 and 4 and tables 1 and 2, where good agreement with experiment and other computations is found.

2.2.2. *Flow over a sphere*

The flow over a sphere was chosen as a validation case since it exhibits Reynolds number sensitivity while being three-dimensional even in the laminar regime. Currently a computation at $Re = 50$ has been completed, and the results are reported here. Although not a complex geometry, the use of unstructured grids allows the problem of polar singularity to be side stepped; the surface of the sphere is paved with quadrilateral elements which are then extruded normal to the sphere surface to generate the volume grid. As shown in Fig. 5, good agreement is obtained with structured-grid computations by Johnson & Patel (1999).

2.2.3. *Flow in a coaxial combustor*

The flow in a coaxial dump combustor geometry has been extensively studied experimentally (Roback & Johnston 1983, Sommerfeld & Qiu 1991) as well as computationally using LES (Pierce & Moin 1998). Data for both cold and reacting flow are available. It is therefore used for validation purposes. Figure 6 shows a cross-section of the geometry. Two cases were considered. Prior to inclusion of the LES model in the code, laminar

	Present results	Computations	Experiments
Drag coefficient	2.01	1.99	2.05
Pressure drag	1.18	–	1.22
Viscous drag	0.83	–	0.83
Separation angle	42.5°	43.8°	41.6°
Min. vel. in bubble	$-0.032U$	$-0.031U$	$-0.040U$
Position of min. vel.	$0.42D$	$0.42D$	$0.36D$

TABLE 1. Comparison to experiments (Taneda 1956, Coutanceau & Bouard 1977, Nieuwstadt & Keller 1973), and computation (Beaudan & Moin 1994) for $Re = 20$.

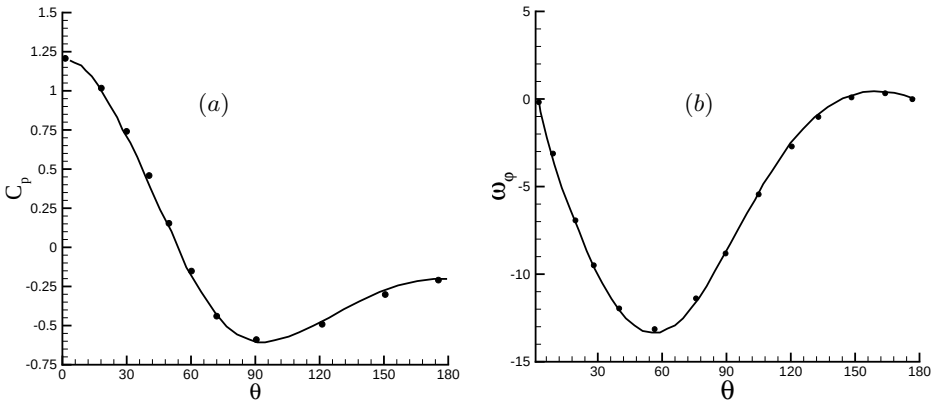

FIGURE 5. The vorticity and pressure coefficient (C_p) on the sphere surface at $Re = 50$ are compared to experimental data. The solid lines are from the calculations, while the symbols are experimental data from Johnson & Patel (1999). (a): C_p, (b): vorticity.

flow in the same geometry was computed. The objective of the laminar calculations was to validate the code by comparing to computations by Pierce (personal communication) using a structured solver in cylindrical coordinates. The three components of the coaxial geometry—core inlet, annular inlet, and test section—were independently considered. The solutions in the inlets are trivial and are not shown here. Figure 7 compares the solution in the test section to results from Pierce, and good agreement is observed.

Currently LES in the same geometry is in progress at conditions corresponding to those of Roback and Johnston, 1983.

2.3. *Flow in a Pratt & Whitney combustor*

Our goal is to perform LES in an industrial gas turbine combustor as part of the overall integrated simulation. A step in that direction is to simulate cold and then reacting flow in an industrial combustor. Pratt & Whitney has provided us with a combustor

	Present results	Computations	Experiments
Drag coeff. (max)	1.329	1.314 - 1.365	1.35
Pressure drag (max)	0.989	1.021	1.01
Viscous drag (max)	0.340	0.344	0.34
Lift. coef. (max)	0.328	0.314 - 0.328	–
Lift coef. (amp)	0.684	0.657	–
Pressure lift (max)	0.290	0.297	–
Viscous lift (max)	0.043	0.045	–
Strouhal no.	0.166	0.164 - 0.166	0.164
$-Cp_{\text{base}}$	0.77	0.73 - 0.74	0.72
$-Cp_{\text{stag.}}$	1.08	1.11	–
Sep. angle	116.1°	117.4°	117.0°

TABLE 2. Flow over a cylinder at $Re = 100$. Comparison to experiments (Williamson 1991, Henderson 1995) and computation (Beaudan & Moin 1994, Mittal (private communication), Kravchenko & Moin 1998).

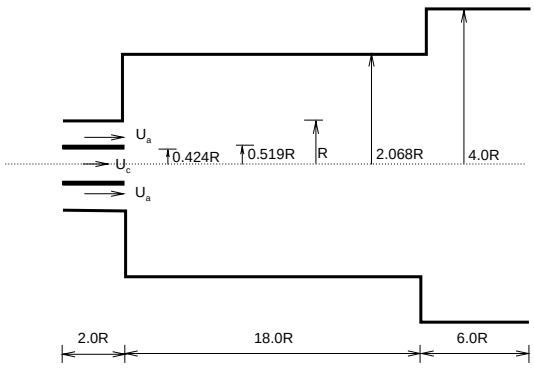

FIGURE 6. Cross-section of coaxial combustor.

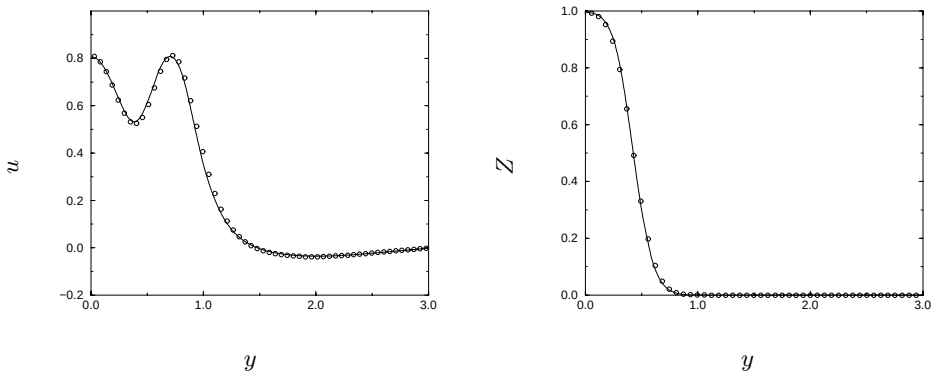

FIGURE 7. Laminar validation in the coaxial combustor geometry. The profiles at $x = 2$ are compared to results from Pierce (private communication) using a structured grid solver. (a): u, (b): Scalar ——— (Pierce), ∘ (present results).

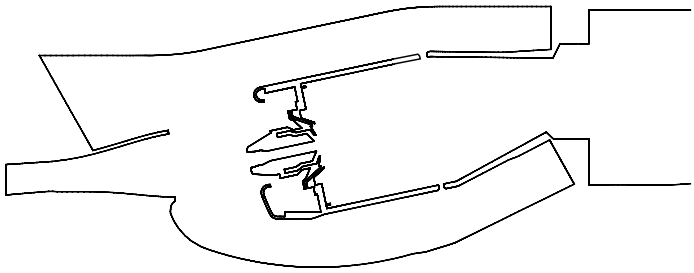

FIGURE 8. Cross-section of combustor.

geometry for which they have data. Simulating flow in the real combustor geometry tests the algorithm and the code as well as our grid generating capability.

Our first step has been to assess our ability to handle the intricate internal details of the combustor geometry and to assess the resolution requirements in the different regions of the flow. Towards that end we have extracted from the original three-dimensional geometry a plane containing important features such as the pre-diffuser, outer diffuser, fuel and air nozzle, and injection holes (Fig. 8). The midplane was extruded in the spanwise direction, and a completely hexahedral grid of about half a million elements was generated. Figure 9 illustrates a portion of the grid.

Plug flow at a Reynolds number of around 3000 was specified at the inlet; the calculations were started from rest and monitored for qualitative accuracy. Figures 10 and 11 show instantaneous streamlines in the pre-diffuser, nozzle, and dilution hole regions respectively. The computation is seen to capture separation, reattachment, and recirculation regions at both large scales (such as in the diffuser and downstream of the nozzle) and small scales (e.g. small corners around the nozzle). Also, the evolution of the flow was tracked, and unsteady details such as starting vortices and separation at sharp edges were seen to be captured. Animation shows a flow that appears periodic and is driven by periodic shedding in the pre-diffuser. This is consistent with the presence of sharp edges and the absence of three-dimensional features.

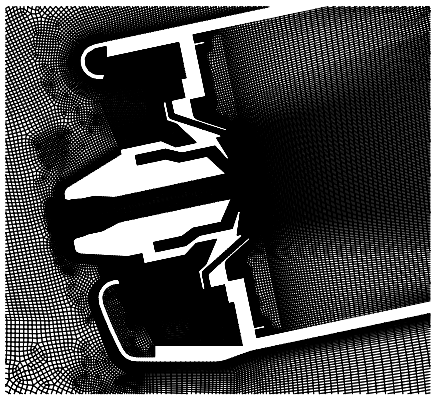

FIGURE 9. A closer view of the grid used in the nozzle.

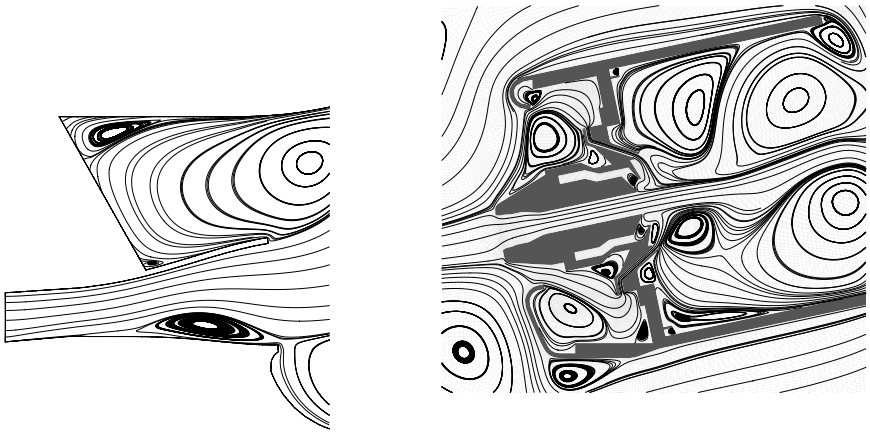

FIGURE 10. Streamlines in the prediffuser and nozzle regions respectively.

Our next step is to generate a suitable grid for the three-dimensional geometry and then simulate scalar mixing in the full configuration.

2.4. *Parallel performance*

The constant density solver was tested on the SGI Origin 2000 and found to scale quite well with the number of processors. Figure 12 shows results from calculations on two different grid sizes, 64000 and 216000 nodes. Note that these grids are quite small as compared to the grids commonly used for turbulence simulations. The computations with 64000 nodes scales linearly almost up to 32 processors, at which point there are only 2000 nodes per processor. The simulations with 216000 nodes is seen to scale linearly far beyond. An empirical rule of thumb used in our calculations is to partition the grid into as few as 5000 elements per processor, should that many processors be available.

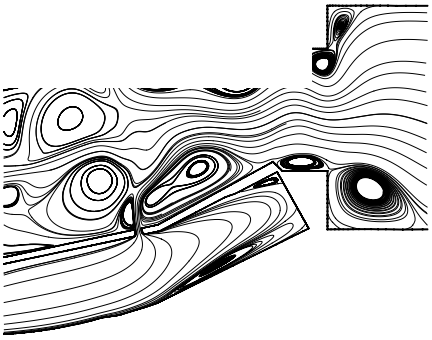

FIGURE 11. Streamlines illustrating flow around the dilution holes.

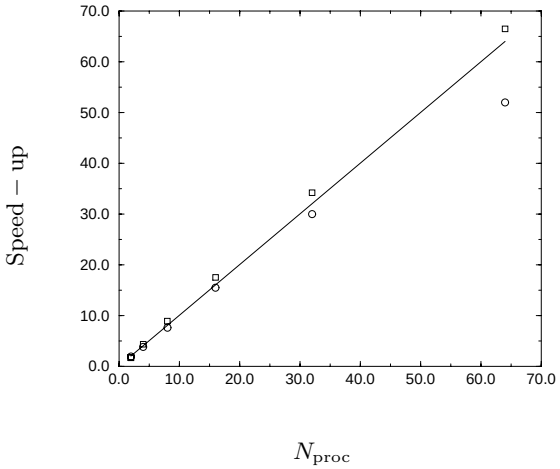

FIGURE 12. Results of a scaling study on the Origin 2000. Two different grid sizes were considered: 64000 nodes (○), and 216000 nodes (□).

3. Summary

This report describes our progress in the last year towards large-eddy simulation of gas turbine combustors. Our progress in the last year is as follows:

• A more efficient version of the constant density algorithm was derived for hybrid grids.

• The constant density algorithm was implemented for hybrid grids, and validated for a variety of steady and unsteady flows.

• Simulations in the Pratt & Whitney geometry have been initiated; the unsteady flow in a subset of the overall geometry was simulated.

• The dynamic Smagorinsky model was extended to unstructured grids, and implemented in the code.

• The algorithm was extended to low Mach number, variable density flows; validation is in progress.
• The spray module is being incorporated.

Acknowledgments

We would like to acknowledge Mr. Gianluca Iaccarino for his expertise and generous help in generating the grids used in our simulations. Financial support for this work is provided by the Department of Energy's ASCI program.

REFERENCES

Akselvoll, K. & Moin, P. 1995 Large-eddy simulation of turbulent confined coannular jets and turbulent flow over a backward facing step. *Report TF-63*, Mechanical Engineering Dept., Stanford University, Stanford, California.

Beaudan, P. & Moin, P. 1994 Numerical investigations on the flow past a circular cylinder at sub-critical Reynolds number. *Report TF-62*, Mechanical Engineering Dept., Stanford University, Stanford, California.

Coutanceau, M. & Bouard, R. 1977 Experimental determination of the main features of the viscous flow in the wake of a cylinder in uniform translation. Part 1. Steady flow. *J. Fluid Mech.* **79**, 231-256.

Germano, M., Piomelli, U., Moin, P. & Cabot, W. H. 1991 A dynamic subgrid-scale eddy viscosity model. *Phys. Fluids A.* **3**(7), 1760-1765.

Ghosal, S., Lund, T. S., Moin, P. & Akselvoll, K. 1994 A dynamic localization model for large-eddy simulation of turbulent flows. *J. Fluid Mech.* **282**, 1-27.

Henderson, R. D. 1995 Details of the drag curve near the onset of vortex shedding. *Phys. Fluids.* (*i*)7(9), 2102-2104.

Kravchenko, A. G. & Moin, P. 1998 B-spline methods and zonal grids for numerical simulations of turbulent flows. *Report TF-73*, Mechanical Engineering Dept., Stanford University, Stanford, California.

Lilly, D. K. 1992 A proposed modification of the Germano subgrid-scale closure method. *Phys. Fluids A.* **4**(3), 633-635.

Meneveau, C., Lund, T. S., & Cabot, W. H. 1996, A Lagrangian dynamic subgrid-scale model of turbulence. *J. Fluid Mech.* bf 319, 353-385.

Nieuwstadt, F. & Keller, H. B. 1973 Viscous flow past circular cylinders. *Computers & Fluids.* **1**, 59-71.

Pierce, C. D. & Moin, P. 1998 Large eddy simulation of a confined coaxial jet with swirl and heat release. *AIAA Paper 98-2892.*

Roback, R. & Johnston, B. V. 1983 Mass and momentum turbulent transport experiments with confined swirling coaxial jets. *NASA CR 168252.*

Sommerfeld, M. & Qiu, H. H. 1991 Detailed measurements in a swirling particulate two-phase flow by a phase-doppler anemometer. *Int. J. of Heat and Fluid Flow.* **12**(1), 20-28.

Taneda, S.1956, Experimental investigation of the wakes behind cylinders and plates at low Reynolds numbers. *J. Phys. Soc. Japan.* **11**, 302.

Williamson, C. H. K. 1996 Vortex dynamics in the cylinder wake. *Ann. Rev. Fluid Mech.* **28**, 477-539.